FORUM ORIGINAL RESEARCH COMMUNICATION

Electrochemical Quantification of Extracellular Local H_2O_2 Kinetics Originating from Single Cells

Monika Bozem,[1] Phillip Knapp,[1] Valentin Mirčeski,[2] Ewa J. Slowik,[1] Ivan Bogeski,[1,3] Reinhard Kappl,[1] Christian Heinemann,[4] and Markus Hoth[1]

Abstract

Aims: H_2O_2 is produced by all eukaryotic cells under physiological and pathological conditions. Due to its enormous relevance for cell signaling at low concentrations and antipathogenic function at high concentrations, precise quantification of extracellular local hydrogen peroxide concentrations ($[H_2O_2]$) originating from single cells is required.

Results: Using a scanning electrochemical microscope and bare platinum disk ultramicroelectrodes, we established sensitive long-term measurements of extracellular $[H_2O_2]$ kinetics originating from single primary human monocytes (MCs) *ex vivo.* For the electrochemical techniques *square wave voltammetry, cyclic* and *linear scan voltammetry,* and *chronoamperometry,* detection limits for $[H_2O_2]$ were determined to be 5, 50, and 500 nM, respectively. Following phorbol ester stimulation, local $[H_2O_2]$ 5–8 μm above a single MC increased by 3.4 nM/s within the first 10 min before reaching a plateau. After extracellular addition of H_2O_2 to an unstimulated MC, the local $[H_2O_2]$ decreased on average by 4.2 nM/s due to degradation processes of the cell. Using the scanning mode of the setup, we found that H_2O_2 is evenly distributed around the producing cell and can still be detected up to 30 μm away from the cell. The electrochemical single-cell measurements were validated in MC populations using electron spin resonance spectroscopy and the Amplex® UltraRed assay.

Innovation and Conclusion: We demonstrate a highly sensitive, spatially, and temporally resolved electrochemical approach to monitor dynamics of production and degradation processes for H_2O_2 separately. Local extracellular $[H_2O_2]$ kinetics originating from single cells is quantified in real time. *Antioxid. Redox Signal.* 29, 501–517.

Keywords: electrochemistry, SECM, ROS, single-cell H_2O_2 quantification, immunology, human monocytes

Introduction

AMONG REACTIVE OXYGEN SPECIES (ROS) relevant for cells, H_2O_2 is probably the most important molecule. It is produced by intra- and extracellular reactions, including the respiratory chain of mitochondria, xanthine oxidases, and NADPH oxidases (NOXs) (16, 24, 52). As major sources of ROS, plasma membrane-residing NOXs produce superoxide radicals ($^{\bullet}O_2^-$) outside the cell by transferring one electron from NADPH, thereby reducing O_2. Due to its charge, $^{\bullet}O_2^-$ does not rapidly diffuse through the plasma membrane into the cytosol, but is almost quantitatively dismutated into H_2O_2 and O_2 ($2\ ^{\bullet}O_2^- + 2\ H^+ \rightarrow H_2O_2 + O_2$). Dismutation occurs spontaneously and is enhanced by the superoxide dismutase

[1]Department of Biophysics, Faculty of Medicine, Center for Integrative Physiology and Molecular Medicine (CIPMM), Saarland University, Homburg, Germany.
[2]Institute of Chemistry, Faculty of Natural Sciences and Mathematics, Ss Kiril i Metodij University, Skopje, Macedonia.
[3]Cardiovascular Physiology, University Medical Center, University of Göttingen, Göttingen, Germany.
[4]HEKA Elektronik Dr. Schulze GmbH, Lambrecht, Germany.

Innovation

Electrochemical methods are tested for quantification of extracellular local concentration of hydrogen peroxide [H_2O_2] kinetics originating from a single cell. With a scanning electrochemical microscope and bare disk platinum ultramicroelectrodes of 10 μm diameter (*vs.* Ag/AgCl), 5-500 nM up to 1 mM [H_2O_2] could be resolved depending on the method. Using chronoamperometry, we performed stable long-term (>3 h) measurements with high temporal (>1 Hz) and spatial (<1 μm) resolution from individual primary human monocytes *ex vivo*. Careful calibrations allow quantification of local extracellular [H_2O_2] in the vicinity of single cells and the separation of H_2O_2 production and degradation by the same cell.

SOD3 (ecSOD) in the extracellular environment (34). Caused by the short $^\bullet O_2^-$ half-life time of around 2 μs (75), direct determination of the $^\bullet O_2^-$ production rate is rather difficult (70). As an indirect quantitative measure of $^\bullet O_2^-$, the more stable H_2O_2 is monitored, which is considered to be the main transmitter of redox signaling (20, 40). To maintain a well-defined redox state of cells, which is an important prerequisite for cellular signaling, a variety of H_2O_2 degradation systems antagonize its production (6, 73). Supported by aquaporin channels, H_2O_2 can diffuse back into the producing cell (5, 11, 27, 36) and, depending on local hydrogen peroxide concentration ([H_2O_2]) and cell density, it can act on neighboring cells. Considering its relevance for many biological processes through oxidation of protein cysteine residues and of other targets (71), quantification of local extracellular H_2O_2 kinetics originating from single cells and separation of H_2O_2 production and degradation are needed to fully explore its physiological roles. Taking intra- and extracellular sources of H_2O_2 into account, sensitive, quantitative, and dynamic measurements of this species in the cell and outside the plasma membrane are required.

To monitor intracellular H_2O_2 on the single-cell level, genetically encoded fluorescent protein sensors such as HyPer or roGFP2-Orp1 (9, 20, 24, 57, 68) and roGFP2-Tsa2ΔCPΔCR (49) can be applied. These sensors provide fascinating insights into intracellular H_2O_2 and its spatial distribution in subcellular compartments. However, there are also drawbacks: problematic calibration, often a limited dynamic range, and interference by pH and by endogenous reductants, as well as light-induced ROS generation (12, 72).

To monitor extracellular H_2O_2 and $^\bullet O_2^-$, Amplex® Red/Amplex® UltraRed assays (41, 57) and electron spin resonance (ESR) spectroscopy (19, 63), respectively, are frequently used. They offer sensitivity in the low nanomolar range, but do not allow single-cell measurements. Extracellular determinations of [H_2O_2] in populations of 10,000 to 100,000 cells per mL have revealed nano- up to low millimolar values (24, 32). However, considering the complex H_2O_2 production and degradation kinetics, these values cannot easily be converted to single cells.

Since a couple of years, sophisticated electrochemical methods have been developed and adapted to selectively determine H_2O_2 from cell populations and single cells (38, 39). Thereby, excellent results for certain individual parameters such as sensitivity or specificity have been obtained [*e.g.*, (2)];

comprehensive measurements of parameters being relevant for the analysis of interrelated physiological processes on the single-cell level, however, have not been reported.

In the present study, we introduce a highly sensitive, spatially, and temporally resolved electrochemical approach to monitor kinetics of H_2O_2 production and degradation from a single cell. Measurements were validated in respective monocyte (MC) populations by a recently modified ESR spectroscopic method (63) and an adapted fluorescence-based Amplex UltraRed assay (47).

Results

Quantification of [H_2O_2] with the scanning electrochemical microscope

The *ElProScan ELP 3* scanning electrochemical microscope (SECM) used for the present study is specified in the Materials and Methods section. For all measurements, ultramicroelectrodes (UMEs) with a bare platinum wire of 10 μm diameter (*vs.* Ag/AgCl) were used, whose electrochemical properties substantially differ from electrodes of larger scales (3, 7, 26). Experiments were performed in phosphate-buffered saline (PBS-I) in ambient air to meet oxygen requirement of living cells. Electrochemically, H_2O_2 can be determined by its reductive ($H_2O_2 + 2H^+ + 2e^- \rightarrow 2H_2O$) or oxidative ($H_2O_2 \rightarrow O_2 + 2H^+ + 2e^-$) electrode reaction. Since reduction of H_2O_2 in a buffer containing O_2 interferes with the oxygen reduction reaction (ORR), leading to additional H_2O_2 (1, 22, 59, 75), anodic oxidation was chosen for H_2O_2 determination.

[H_2O_2] calibration by cyclic voltammetry and linear scan voltammetry. To define the respective redox potential under our experimental conditions, cyclic voltammetry (CV) was analyzed in a potential window of -100 mV up to +1.0 V at a scan rate of 50 mV/s in the absence (blank current; black traces in Fig. 1A) or the presence of 20 μM [H_2O_2] (red trace). Current values specifically increased with increasing [H_2O_2] at a potential range of 500 to 650 mV, which is in agreement with the peak potential for anodic oxidation of H_2O_2 at 650 mV (39, 67). Consequently, in CV and linear scan voltammetry (LSV) (Fig. 1A, B), current values were sampled at 650 mV (I_{650}) and chronoamperometric (CA, see the [H_2O_2] calibration by chronoamperometry section) experiments were conducted at 650 mV (Fig. 1C). Current values (I_{650}) linearly increased by 3.3 $\pm$ 0.06 pA for CV (Fig. 1D, red line) and by 3.7 $\pm$ 0.11 pA for LSV per μmol of H_2O_2 (Fig. 2E, red line). As explained in the Materials and Methods section, the starting potential of the CV and LSV determines the slope of the linear regression. Starting at +100 mV revealed almost no current change with increasing [H_2O_2] (blue lines in Fig. 1D, E), whereas starting at -1.0 V was followed by the steepest slope (black lines in Fig. 1D, E). This can be explained by additional electrochemical production of H_2O_2 due to the ORR (see the Materials and Methods section). Red-colored traces in Figure 1D and E were obtained with a starting potential at -100 mV where cleaning of the UME is expected (compare the Materials and Methods section).

To summarize, in CV and LSV calibration experiments, [H_2O_2] from 500 nM up to 1 mM could be resolved. At lower scan rates of 20, 10, or 5 mV/s, but with reduced temporal resolution, [H_2O_2] down to 50 nM was detectable (the scan rate of 20 mV/s shown in the inset of Fig. 1A, red trace).
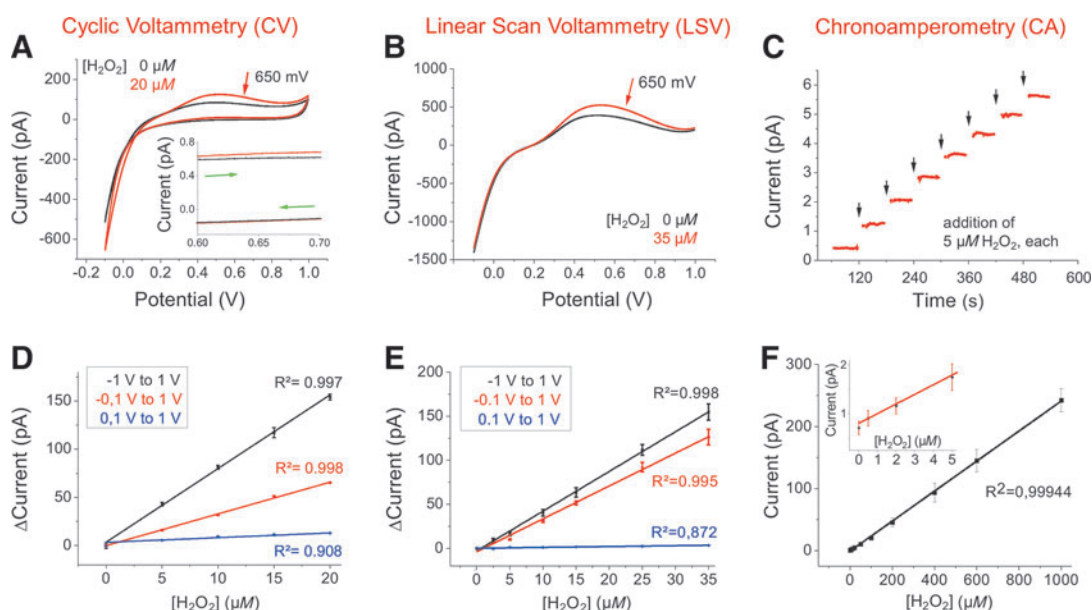
FIG. 1. **[H$_2$O$_2$] calibration with different electrochemical techniques.** Experiments were conducted in PBS-I buffer, using a 10 μm Pt-UME *versus* Ag/AgCl. **(A)** CVs with 0 (*black*) and 20 μM H$_2$O$_2$ (*red*). Potential window from -0.1 to +1.0 V; scan rate 50 mV/s. In the *inset* (potential window of 0.6–0.7 V at a larger scale), the lower detection limit for [H$_2$O$_2$] of 50 nM (*red trace*; *black trace* 0 H$_2$O$_2$) at a scan rate of 20 mV/s is exemplified. *Green arrows* indicate forward and backward directions of cycling. **(B)** LSVs with 0 (*black*) and 35 μM H$_2$O$_2$ (*red*). Forward scanning was conducted from -0.1 to +1.0 V at a scan rate of 50 mV/s. Then, potential was reduced in one quick step to -0.1 V, clamped for 3 s, before forward scanning started again. **(C)** Representative CA measurement at 650 mV under pulsed additions of H$_2$O$_2$ (5 μM steps; *arrows*) to cell-free buffer (example for *n* = 10 similar experiments). **(D)** Current–dose relationship for H$_2$O$_2$ measured in CV at different potential windows described in the *box* (scan rate 50 mV/s). *ΔI* values represent current values sampled at 650 mV subtracted by respective basal current values of the CV before addition of H$_2$O$_2$. For each experiment with different potential window and/or different [H$_2$O$_2$] current values (*ΔI$_{650}$*) of sweep numbers 2–10 were averaged. Mean ± SEM (*n* = 5) is shown. **(E)** Current–dose relationship for H$_2$O$_2$ measured in LSV at different potential windows described in the *box* [scan rate 50 mV/s; protocol as in **(B)**]. Current values (*ΔI$_{650}$*) were analyzed as for CVs in **(D)**. Mean ± SEM (*n* = 4) is shown. **(F)** Current–dose relationship measure in CA for [H$_2$O$_2$] from 500 nM to 1 mM (cell free, *n* = 10; *red inset n* = 3 for [H$_2$O$_2$] of 0–5 μM). For calculations, current values (*I$_{650}$*) of the respective approximate linear steady-state phase after each H$_2$O$_2$ addition were averaged. Mean ± SEM is shown. CA, chronoamperometric; CV, cyclic voltammogram or cyclic voltammetry; [H$_2$O$_2$], local hydrogen peroxide concentration; LSV, linear scan voltammogram; UME, ultramicroelectrode.

[H$_2$O$_2$] calibration by chronoamperometry. Steady-state conditions, where the current measured with UMEs is purely faradaic with no capacitive component, are ideally met during CA experiments at a fixed potential. For calibration, H$_2$O$_2$ was added to the PBS-I buffer to reach final concentrations of 5 μM or multiples of it (Fig. 1C). Calibrations were performed in the presence of attached human MCs at the end of each experiment. The UME was fixed at least 1 mm above the cell layer to avoid local effects from the cells. Under these conditions, currents increased on average by 224 ± 12.4 fA per μmol of H$_2$O$_2$ (*n* = 25). In cell-free PBS-I, the resulting calibration factor of 233.6 ± 20 fA per μmol of H$_2$O$_2$ (*n* = 10; Fig. 1F) was not significantly different. To determine the lowest [H$_2$O$_2$] measurable with CA, [H$_2$O$_2$] of a cell-free PBS-I buffer was increased stepwise by 100 nM. As shown in the red inset of Fig. 1F, 500 nM [H$_2$O$_2$] could be distinguished from blank buffer. For [H$_2$O$_2$] higher than 1 mM, calibrations did not provide reliable data (not shown), in agreement with findings of *Urbach and Bowen* (65) and *Zhang and Wilson* (74).

The CA calibration for [H$_2$O$_2$] was linear over more than three orders of magnitude from 500 nM up to 1 mM (Fig. 1F). Considering the signal-to-noise ratio of a typical UME and

the calibration value of 224 ± 12.4 fA per μmol of H$_2$O$_2$, a concentration of 500 nM can thus be reliably measured in CA.

[H$_2$O$_2$] calibration by square wave voltammetry. Finally, square wave voltammetry (SWV) was tested for its applicability to measure [H$_2$O$_2$] in the nano- to millimolar range (Fig. 2). This technique combines chronoamperometric with pulsed voltammetric components (44–46). SWV was reported to be superior to other voltammetric methods, mainly due to enhanced sensitivity for analytical determinations, but has not been applied to measure low [H$_2$O$_2$] with UMEs (44). The principle of SWV is described in detail elsewhere (44). In brief, anodic oxidation of H$_2$O$_2$ was used for its determination within a potential window from -100 up to +900 mV. Oppositely directed potential steps of 1 s duration each, along a staircase ramp, were applied repetitively to values 75 mV above and below the mean potential line and thus reached anodic oxidation of H$_2$O$_2$ already at a mean potential between 470 and 500 mV. Potential was increased over time by an increment of 10 mV, set on top of each positively directed potential step (scan rate = 5 mV/s). Figure 2A shows a current trace resulting from one potential step pair. The initial peaks
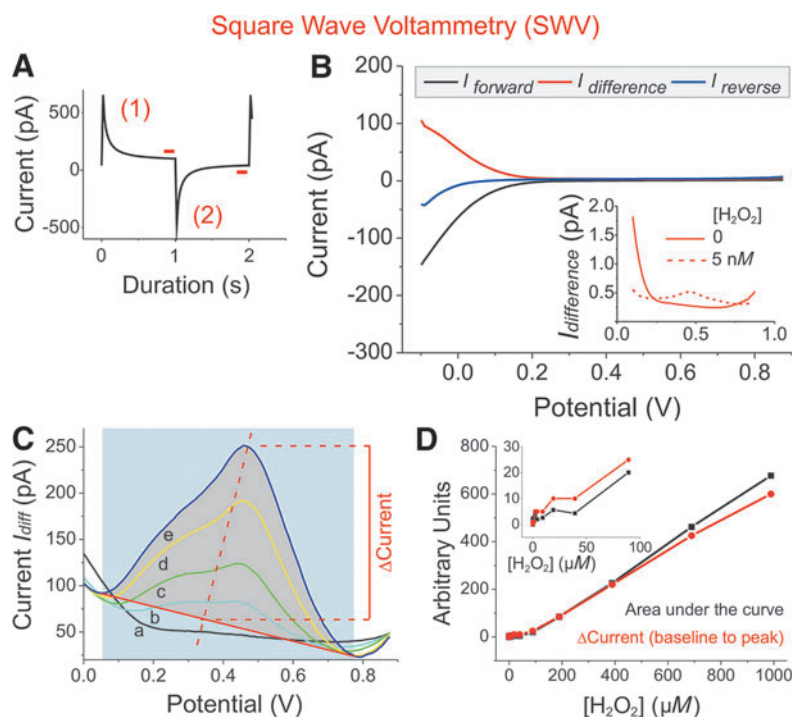
FIG. 2. H₂O₂ determination by SWV. Experiments were performed in PBS-I buffer, using a $10\,\mu m$ Pt-UME *versus* Ag/ AgCl. **(A)** SWV is a repetitive double-step chronoamperometric technique. For each double-step, two equal, but oppositely directed, potential pulses (± 75 mV) were generated, the duration of which was set to $\tau = 2$ s. In a potential window from -0.1 up to +0.9 V mean (nominal) voltage was increased over time by an increment of 10 mV set on top of each positively directed potential step (scan rate = 5 mV/s). Values of the anodic forward (1) and cathodic reverse current (2) were sampled and averaged from the last 10% of the respective plateau phase (*red bars*). **(B)** Current traces of a representative SWV experiment in blank buffer. For the net current ($I_{difference}$; *red traces*), $I_{reverse}$ (measured during the negatively directed potential steps; *blue* trace) was subtracted from $I_{forward}$ (measured during the positively directed steps; *black trace*). The *inset* with a potential window from 0.1 to 0.9 V shows the characteristic change in the current trace ($I_{difference}$) at a mean potential between 470 and 500 mV after H₂O₂ to a final concentration of 5 nM had been added (*dotted line*). **(C)** For calibrating current changes to [H₂O₂], maxima of $I_{difference}$ were determined for different [H₂O₂] (in μM: 990: e, *dark blue*; 690: d, *yellow*; 390: c, *green*; 190: b, *light blue*; 0: a, *black*). After definition of a baseline (*solid red line*), Δcurrent ($I_{peak} - I_{baseline}$) was calculated. Alternatively, the size of the area under the curve (*gray*) was determined. As an example, analysis for the *dark blue curve* **(e)** is shown. **(D)** Δcurrent and area under the curve as determined in **(C)** were normalized to each other and plotted in arbitrary units against [H₂O₂]. The *inset* shows a magnification at lower [H₂O₂]. SWV, square wave voltammetry.

of charging current quickly decline to reach the respective stable plateau. Values of the anodic forward (red-colored 1) and cathodic reverse current (red-colored 2) were sampled and averaged from the last 10% of the respective plateau phase (Fig. 2A, red bars).

In Figure 2B, current traces from a representative SWV experiment are depicted. For the net current ($I_{difference}$; red traces), values from $I_{reverse}$ (cathodic current; blue trace) were subtracted from those of $I_{forward}$ (anodic current; black trace) according to $I_{difference} = I_{forward} - I_{reverse}$. For analysis of the current–dose relationship for H₂O₂, values of $I_{difference}$ were compared at a potential interval from 0 to +900 mV, where H₂O₂ oxidation-induced current changes are expected. The inset in Figure 2B reveals the characteristic change of $I_{difference}$ at a mean potential between 470 and 500 mV after H₂O₂ had been added to the buffer. At the given scan rate of 5 mV/s, [H₂O₂] of 5 nM could be resolved (Fig. 2B, inset).

Methods to analyze SWV experiments (Fig. 2C, D) are detailed in the Materials and Methods section. In brief, first the baseline of a peak current curve ($I_{difference}$) is defined (solid red line in Fig. 2C). Then, the area under the curve (gray) is determined by integration or, as an alternative, ΔI is

calculated from the baseline to the peak of the curve (Fig. 2C). Both approaches turned out to be equally valid for SWV calibration of [H₂O₂] (Fig. 2D).

In summary, with SWV, [H₂O₂] from 5 nM up to 1 mM could be measured, making it the most sensitive method with the largest concentration range of six orders of magnitude.

Buffering capacity of PBS-I – pH measurements. H₂O₂ is known to chemically act as a weak acid and, by pH changes, may modify electrochemical properties of the measuring solution. To test the buffering capacity of PBS-I used in all electrochemical experiments, [H₂O₂] was increased stepwise to reach final concentrations of 1 up to 5 mM in the stirred buffer solution. Simultaneous pH measurements revealed stability of the starting pH value at 7.37 over the whole experiment and a wide range of [H₂O₂] (see Fig. 4A).

Effect of glucose in the buffer. Since glucose is required as a nutrient for living cells and as a prerequisite of H₂O₂ production in human MCs (51), we compared the H₂O₂ measurements in the absence and presence of 5 mM glucose in cell-free PBS-I. Neither with the voltammetric techniques

(CV, LSV, or SWV) nor during CA measurements did glucose show any electrochemical effect [not shown; (35)].

Quantification of H$_2$O$_2$ generated by single human MCs

MCs are white blood cells (leukocytes) that fulfill important functions for innate immunity. They can differentiate into macrophages (MPhs) that eliminate bacteria and other pathogens by phagocytosis (50, 60, 64). MCs and MPhs are known to produce high amounts of ROS intra- and extracellularly. The major sources for external ROS are NADPH oxidases (NOXs), which are located in the plasma membrane (37, 52). In human MCs, NOX2 is the main $^{\bullet}$O$_2$- and thus H$_2$O$_2$-generating enzyme complex (57).

Artificial NOX activation by the phorbol ester 12-*O*-tetradecanoylphorbol-13-acetate (TPA) causes MCs to produce $^{\bullet}$O$_2^-$, which is dismutated to H$_2$O$_2$. Using CA at 650 mV, current was measured with the UME placed 5–8 μm above a single MC (Fig. 3C). Using this technique, only local current changes (ΔI_{650}) within an active volume around the cell and the UME are monitored, which might be completely different from the electrochemical situation in the unstirred bulk solution. Increasing the gap between the UME and the H$_2$O$_2$-producing cell is followed by a decrease in ΔI reaching $\Delta I = 0$ at a distance of ≥ 1 mm (not shown).

As shown in Figure 3A, the solvent for TPA, dimethyl sulfoxide (DMSO), caused a small and transient electrochemical artifact. Following TPA application, a significant rise in current was measured above the MC reflecting a rise in [H$_2$O$_2$].

To test, if in addition to H$_2$O$_2$ other reactive oxygen or nitrogen species are also released by a TPA-stimulated MC, species which possibly would modify the H$_2$O$_2$ determination at the given potential (2), we performed several control experiments (Fig. 4). First, superoxide dismutase (SOD) was applied on top of TPA after H$_2$O$_2$ production of the cell had reached the plateau phase (Fig. 4B). Since no change of current was observed, we conclude that $^{\bullet}$O$_2^-$ is not determined at 650 mV and, in addition, $^{\bullet}$O$_2^-$ produced at the plasma membrane is quickly and quantitatively dismutated to H$_2$O$_2$. Furthermore, MCs were pretreated for 30 min with VAS2870 in DMSO, a cell-permeable *pan* NOX inhibitor (Fig. 4C, D, red). This treatment completely prevented the TPA-induced current rise (only the small DMSO artifact was left). Application of external H$_2$O$_2$ (5 μM), however, resulted in the usually observed current increase. Control cells of the same batch, but pretreated with DMSO instead of VAS2870, responded to TPA stimulation with H$_2$O$_2$ production (Fig. 4C, black trace; Fig. 4D, gray column). We conclude that the current increase exclusively reflects an increase in [H$_2$O$_2$] due to NOX enzyme activity.

To test for production of other radicals besides $^{\bullet}$O$_2^-$, ESR spectroscopy was applied (Fig. 4E, F). We analyzed signals
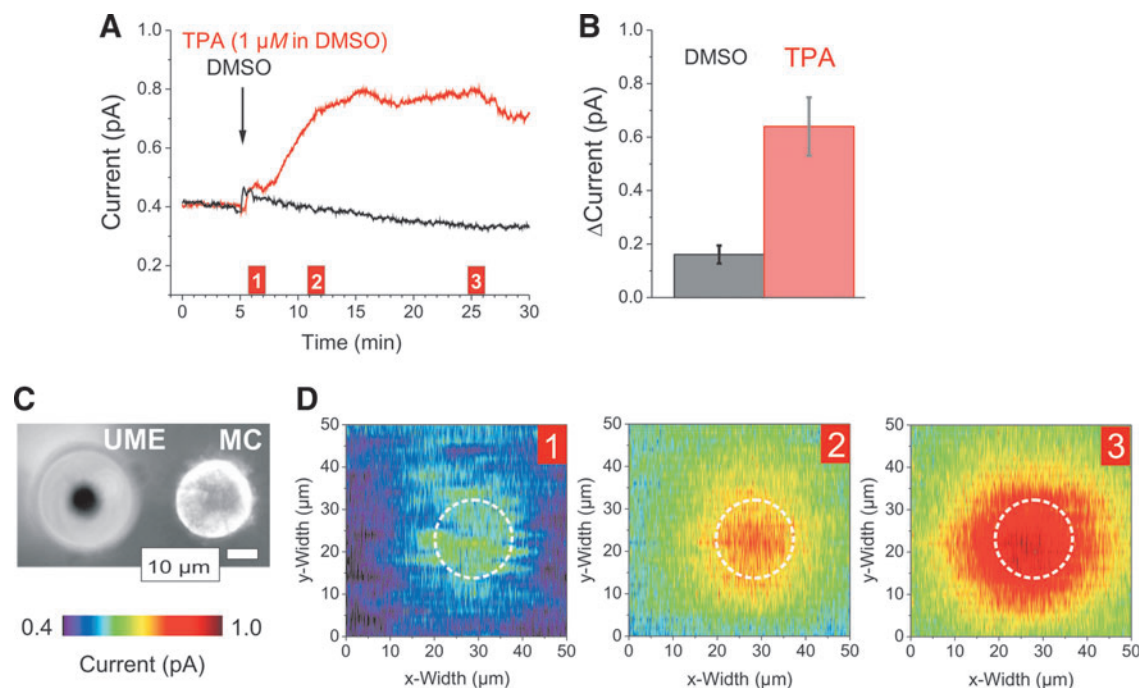

FIG. 3. H$_2$O$_2$ measurements from single MCs after stimulation with the phorbol ester TPA. CA experiments were conducted at 650 mV in PBS-I buffer. A 10 μm Pt-UME (*vs.* Ag/AgCl) was placed 5–8 μm above different individual MCs in the experiments shown in **(A)** and **(D)**. **(A)** CA measurement of a single MC after stimulation with TPA (*red trace*). The solvent DMSO (0.2%) was used in a control experiment with the same cell, but preceding TPA stimulation (*black trace*). **(B)** Average total current increase (±SEM) of single cells as shown in **(A)** after application of DMSO (161 ± 33.6 fA; *n* = 25) or TPA stimulation (639.8 ± 108.8 fA; *n* = 23). **(C)** Bright-field image of an MC and the tip of the UME. **(D)** Three consecutive 2D scans after TPA stimulation of the MC shown in **(C)** whose position is marked by *dashed white circles*. Numbers in the *right upper corners* refer to the time points indicated in **(A)** where another exemplary MC was measured. 2D scan images **(D)** are representative for *n* = 17 different scanning experiments with individual cells. Settings: constant height; scanning rate *x* = 2 μm/s, 50-nm resolution; *y* = 2 μm, alternate mode; raw data, no compression. MC, monocyte; TPA, 12-*O*-tetradecanoylphorbol-13-acetate.
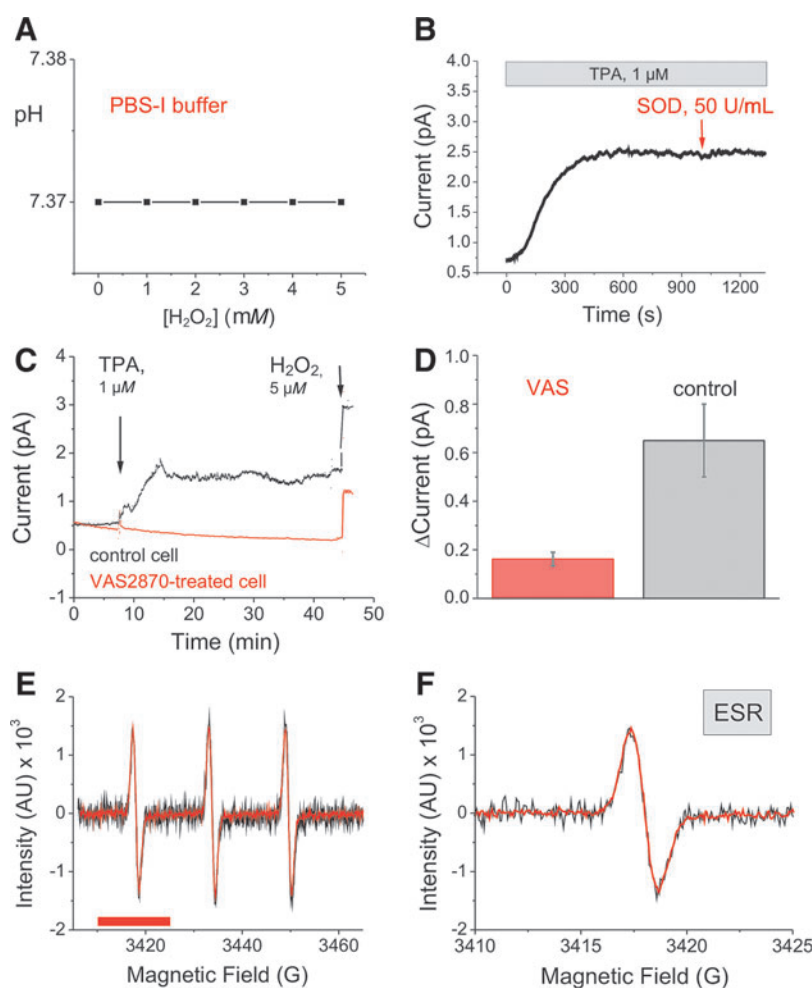
FIG. 4. Control experiments. (A) pH measurements in PBS-I before and after addition of 1 to $5\,mM$ H_2O_2 ($n=3$). **(B)** and **(C)** Single-cell chronoamperometric experiments (at $650\,mV$) with a $10\,\mu m$ Pt-UME *versus* Ag/AgCl in PBS-I with the electrode fixed 5–$8\,\mu m$ above the MC. **(B)** Addition of SOD ($50\,U/mL$) to a TPA-stimulated MC (example for $n=3$). **(C, D)** TPA stimulation of MCs pretreated either with the *pan* NOX inhibitor VAS2870 ($20\,\mu M$ in DMSO; $30\,min$; *red trace*) or with DMSO (*black trace*; examples for $n=5$ per condition). **(E, F)** Comparison of normalized ESR spectra from experiments with MC suspensions (depicted in Fig. 7D, E) to test for $NO^\bullet$ formation by TPA-stimulated MCs. Experimental conditions and settings of the ESR spectrometer are detailed in the Materials and Methods section. *Black traces* are from DMSO treated (control; $n=3$) and *red traces* from cells about $35\,min$ after TPA application ($n=3$). Spectra in **(E)** and the enlarged cut out in **(F)**, corresponding to the magnetic field interval marked by the *red bar* in **(E)**, show complete overlay of the normalized spectra. Because of the low intensity, the signal-to-noise ratio of the spectra from unstimulated MCs is higher than from stimulated cells. ESR, electron spin resonance; SOD, superoxide dismutase.

from TPA-stimulated MCs (red traces in Fig. 4E, F) and signals of unstimulated controls (black traces in Fig. 4E, F). Because of $^\bullet O_2^-$ production, signal intensity from TPA-stimulated MCs was higher than signal intensity of control cells. Following normalization of different intensities, ESR spectra could be plotted on top of each other (Fig. 4E, F). Highly diffusible radicals (such as $NO^\bullet$ and $NO_2{}^\bullet$) should modify the line width of the spectra. As this was not the case, we conclude that measurable amounts of additional radicals (*e.g.*, $NO^\bullet$) were not produced. If minimal quantities of $NO^\bullet$ would be generated constitutively or after TPA stimulation, this species would effectively react with $^\bullet O_2^-$ to form $ONOO^-$ (peroxynitrite). It cannot be excluded that $ONOO^-$ is also trapped at a potential of $650\,mV$ (2). However, since $NO^\bullet$ could not be detected, $[ONOO^-]$ should be much lower than $[^\bullet O_2^-]$ and $[H_2O_2]$ if present at all. Thus, $ONOO^-$ signals should not compromise H_2O_2 measurements. Collec-

tively, our experiments indicate that current changes (ΔI_{650}) induced by TPA-stimulated MCs reflect changes in $[H_2O_2]$.

The extracellular distribution of H_2O_2 released from a single cell is highly relevant not only for the producing cell but also to its neighboring cells. Therefore, we used the scanning option of the setup to monitor the spatial distribution of H_2O_2 being continuously delivered by an MC into its immediate vicinity. Only those MCs were scanned that had no neighboring cells in the periphery to exclude the interference by other MCs. For scanning purposes, the position of the UME was fixed (constant height mode) and the table with the cell dish was automatically moved following a predefined protocol. Three consecutive 2D scans from the MC pictured in Figure 3C are presented in Figure 3D corresponding to the time points indicated in Figure 3A. The activity profiles show that H_2O_2 is rather evenly distributed all over the cell, resembling similar levels as shown in Figure 3A (from a

different MC). Due to diffusion, H_2O_2 forms a concentration gradient around the cell and is detectable at least 20 μm away from it in this example. Thus, H_2O_2 generated by one cell could easily influence neighboring cells.

H_2O_2 quantification. TPA-stimulated single MCs as the one depicted in Figure 3A produced a total current increase (ΔI_{650}) of 639.8 ± 108.8 fA ($n = 23$) compared with 161.0 ± 33.6 fA by the solvent DMSO ($n = 25$; Fig. 3B). Maximal current values were reached 23.5 ± 4.2 min ($n = 17$) after TPA application. Subtracting the DMSO artifact, maximal ΔI of 639.8 fA – 161.0 fA = 478.8 fA was measured in the 23 cells treated as the one in Figure 3A. Since current changes in single-cell experiments as well as in calibration experiments are measured in the same volume of solution around the UME tip, current–dose calibrations for H_2O_2 can be applied to determine its concentration in cell experiments. Using the cali-

bration factor for CA experiments of 224.0 ± 12.4 fA/μmol of H_2O_2, an increase of ΔI by 478.8 fA reflects a maximal [H_2O_2] of 2.1 μM in the immediate vicinity of the producing MC. Considering that this concentration is reached on average 23.5 min after TPA application, the net increase in [H_2O_2] caused by a single cell per second is approximately 1.5 nM in the local volume at the UME tip.

Applying the same conditions as in the CA measurements (Fig. 3A), we repeated the experiments with CV. For this purpose, the UME was positioned 5–8 μm above an MC. Cycling in a potential window from -100 mV up to +1.0 V at a scan rate of 20 mV/s was repeated for >1 h. After 10 min of equilibration in blank buffer, cells were challenged with TPA (1 μM). Current changes at 650 mV (ΔI_{650}) within the first 30 min after TPA stimulation were quantified and the respective calibration for CV of 3.3 ± 0.06 pA per μM H_2O_2 (see Fig. 1) was applied. We found an average local [H_2O_2]
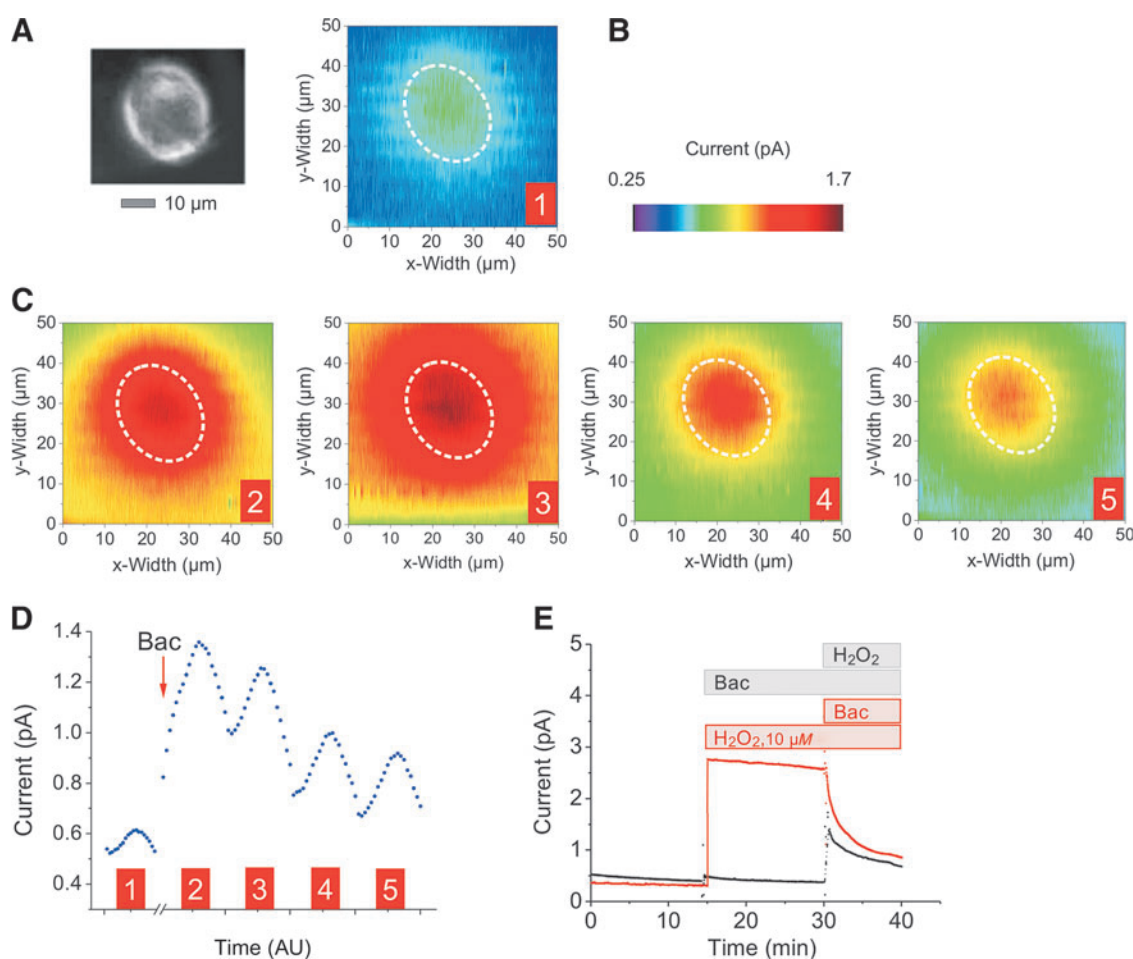

FIG. 5. Respiratory burst of an MC after stimulation with *Escherichia coli*. 2D scans (**B, C**) of the cell in (**A**) and control experiments (**E**) were performed chronoamperometrically at 650 mV in PBS-I buffer using a 10 μm Pt-UME *versus* Ag/AgCl. (**B, C**). With the UME placed 5–8 μm above, the MC shown in (**A**) was measured in five consecutive 2D scans before (**B**) and after addition (**C**) of a cell-free *E. coli* supernatant in *LB* medium (Bac). *Dashed white circles* mark the position of the MC (**A**) during the scanning procedure. Scan settings: constant height; scanning rate $x = 2$ μm/s, 50-nm resolution; $y = 2.5$ μm, alternate mode; raw data, no compression. To complete one 2D scan, 8.5 min were needed. (**D**) *Dotted blue traces* quantify current values of the five 2D scan images in (**B**) and (**C**); numbers of waves 1–5 refer to the corresponding 2D scan numbers. Each 2D scan comprises 20 scan lines alternating in the x-direction, separated by 2.5 μm in the y-direction (meander scan). The mean current value of each scan line of the five 2D scans (5*20 scan lines = 100 mean values) is represented by one *blue dot* (**D**). (**E**) Control experiments (representative of $n = 8$ per condition). Addition of bacterial supernatant [Bac; same amount as in (**C**)] to blank PBS-I (*black trace*) and to PBS-I containing H_2O_2 (10 μM; *red trace*).

increase of 1.3 nM per second ($n = 7$; not shown) in very good agreement with the CA experiments. We conclude from the CV and CA experiments that a TPA-stimulated human MC increased extracellular local [H$_2$O$_2$] on average by 1.4 nM per second.

H$_2$O$_2$ production of MCs stimulated by Escherichia coli bacteria - respiratory burst

TPA is a commonly used nonphysiological stimulus for human MCs. To mimic physiological conditions, MCs were exposed to a cell-free supernatant from cultured *Escherichia coli* bacteria. The supernatant contains bacterial signal peptides that activate formyl peptide receptors in the plasma membrane of the MC (17). Thereby, an intracellular signaling cascade is initiated, which results in the so-called respiratory burst. The respiratory burst is an important part of the complex innate immune response to bacterial pathogens and includes high consumption rate of oxygen coupled to H$_2$O$_2$ production (23, 30, 43). Other components of the bacterial supernatant may also directly activate NOX2 (54).

An aliquot of the supernatant (1:100 vol/vol; final [protein] of 110 μg/mL) was applied to cells in the measuring buffer and five consecutive 2D scans were taken from the individual MC depicted in Figure 5A. Each scan comprises 20 scan lines, one line in the positive, alternating with one line in the negative *x*-direction, but always separated by 2.5 μm in the *y*-direction. Scanning of the area of 50 × 50 μm at a velocity of 2 μm/s required 8.5 min per scan. Starting from low basal activity (Fig. 5B), the cell responded with a respiratory burst characterized by a fast and huge increase of current, which gradually declined (Fig. 5C). The series of five 2D scan images shows the example of one individual MC. The decline of current with time can be explained by a combination of H$_2$O$_2$ diffusion, degradation in- and outside the cell (see the Quantification of H$_2$O$_2$ degraded by single human MCs section), and fast desensitization of the formyl peptide receptors (17).

The traces in Figure 5D average the current from five 2D scans shown in Figure 5B and C. Each blue dot in Figure 5D represents the mean current of one scan line; the numbers of the five waves in Figure 5D refer to the respective scan numbers in Figure 5B and C. The traces reflect the characteristic dynamics of [H$_2$O$_2$] changes during the respiratory burst of a single MC.

In control experiments, addition of the appropriate amount of bacterial supernatant (Bac) or pure *LB* medium to cell-free PBS-I buffer did not change the current flow (Fig. 5E, black trace). In the presence of 10 μM H$_2$O$_2$, however, the supernatant (Bac) as well as the *LB* medium caused reduction of current by the same amount (Fig. 5E, red trace). As a consequence, in experiments applying bacterial supernatant in *LB* medium, current values of the respiratory burst are underestimated and [H$_2$O$_2$] concentrations should be even higher than reported here.

Quantification of H$_2$O$_2$ degraded by single human MCs

As depicted in Figure 3A for a single TPA-stimulated MC, the initial local [H$_2$O$_2$] increase (measured 5–8 μm above the MC as a rise in ΔI) can be higher than the mean increase while approaching a steady-state level. Within the first 10 min after TPA application, the average local [H$_2$O$_2$] change was 3.4 nM per second ($n = 13$). Such a change in production kinetics was observed in most cells and subsequently [H$_2$O$_2$] declined, although the stimulus was still present. It can be excluded that the decline is caused by NADPH- or O$_2$ depletion of the cell since the experiments
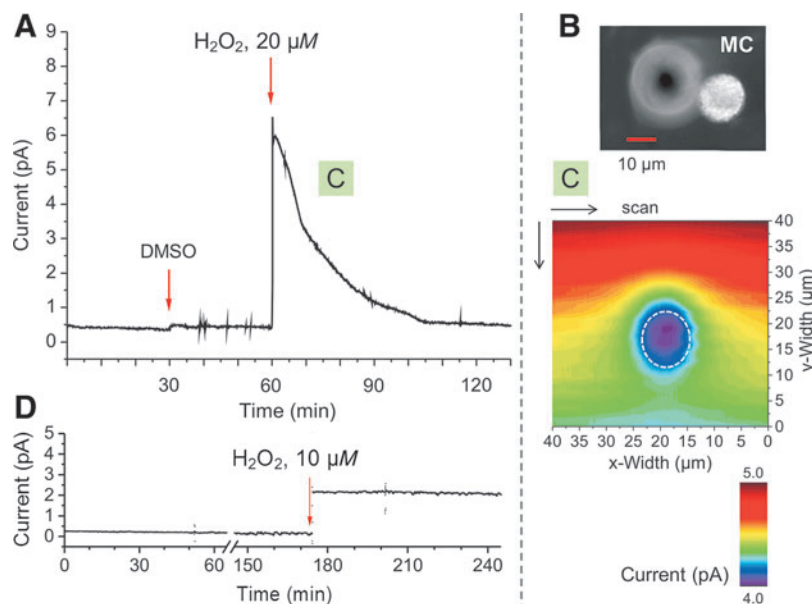

FIG. 6. Degradation of extracellular applied H$_2$O$_2$ by single MCs. CA experiments were conducted at 650 mV in PBS-I buffer using a 10 μm Pt-UME *versus* Ag/AgCl. The UME was placed 5–8 μm above the MC. **(A)** An MC was challenged first with the solvent DMSO (0.2%) and 30 min later with H$_2$O$_2$ (20 μM). **(B)** A different MC was treated in the same way as described in **(A)**, and then a 2D scan was started 5 min after H$_2$O$_2$ application [**C**, *green square* corresponds to the time point in **(A)**]. The *dashed white circle* marks the position of the MC **(B)** during scanning procedure. Scan settings were the same as in Figure 3. **(D)** A cell-free control CA experiment over more than 4 h in the absence or presence of H$_2$O$_2$ ($n = 3$).

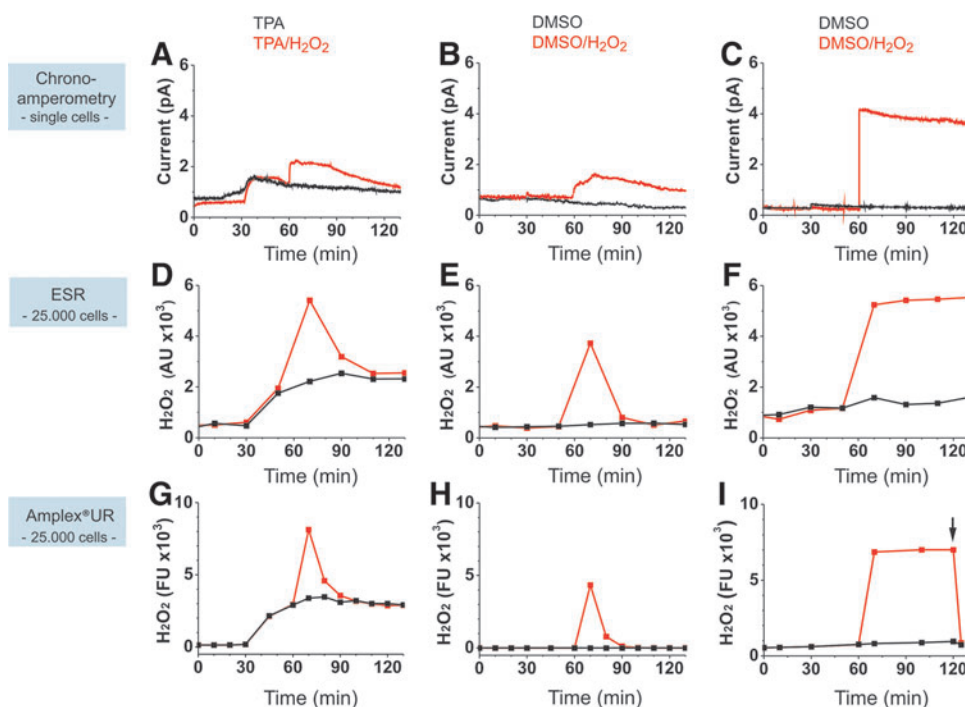**FIG. 7.** **H$_2$O$_2$ production and degradation by MCs: validation of single-cell measurements using the *ElProScan* with cell population measurements by ESR and an AUR assay. (A, B)** Chronoamperometric (CA) measurements of single MCs ($n = 5$–11) with a 10 μm Pt-UME *versus* Ag/AgCl. **(C)** Control in cell-free PBS-I ($n = 4$). **(D, E)** Cell population measurements with ESR ($n = 3$). **(F)** Control in cell-free PBS-I ($n = 3$). **(G, H)** Cell population measurements with the fluorescence-based AUR assay ($n = 3$). **(I)** Control in cell-free PBS-I ($n = 11$). For each approach in **(A–I)**, one representative experiment is shown; results for ESR and AUR are expressed in arbitrary/fluorescence units (AU and FU, respectively). While CA measurements were conducted continuously (1 Hz sampling rate), in ESR- and AUR experiments, H$_2$O$_2$ was determined at selected time points for a pool of 25,000 cells each. Protocol for all experiments: 1 μM of the phorbol ester TPA (or its solvent DMSO, 0.2%) was applied 30 min after the initial equilibration phase. Thirty to 40 min later, either H$_2$O$_2$ (10 μM) or A. dest. was added. The same protocol was followed for cell-free control experiments shown in **C, F, I**, with TPA being replaced by DMSO. **(A, D, G)** TPA-stimulated cells with (*red*) and without (*black*) further treatment with H$_2$O$_2$. **(B, E, H)** Unstimulated cells challenged with H$_2$O$_2$ (*red*) or A. dest. (*black*). **(C, F, I)** Cell-free control experiments with DMSO and H$_2$O$_2$ (*red*) or A. dest. (*black*). AUR control experiments were terminated by addition of catalase (100 U/mL; *arrow*) to test the assay for selectivity to H$_2$O$_2$. AUR, Amplex® UltraRed.

were conducted in a glucose-containing buffer and in the presence of O$_2$. However, multiple extra- and intracellular mechanisms are known to be responsible for H$_2$O$_2$ breakdown (5, 21, 66).

To monitor H$_2$O$_2$ degradation by single cells *ex vivo*, a bolus of H$_2$O$_2$ was applied to unstimulated MCs. The CA measurement from a single cell revealed a decay of [H$_2$O$_2$] from 20 μM to baseline in about 50 min in the example shown (Fig. 6A). In this case, degradation was quite fast; some other MCs showed slower response (compare, for instance, Fig. 7B). This variability was found to be specific for individual cells and not influenced by surrounding cells. Making use of the scanning mode of the setup, another MC (Fig. 6B), having been treated similarly as the one in Figure 6A, was scanned 10 min after H$_2$O$_2$ application. Since our setup scans a selected area from the lower right to the upper left corner, we have turned the scan image in Figure 6C by 180° to visualize the [H$_2$O$_2$] decrease over time corresponding to Figure 6A. Figure 6C shows that [H$_2$O$_2$] above and in close vicinity of the cell (blue area) was markedly reduced within a few minutes. It is assumed that extracellular H$_2$O$_2$ diffuses into the cell and is effectively degraded intracellularly. Results from both,

Figure 6A and C, impressively visualize how MCs can function as a sink for H$_2$O$_2$.

In control experiments (Fig. 6D; $n = 3$) performed in cell-free PBS-I, current values were stable over 4 h in the absence as well as in the presence of 10 μM H$_2$O$_2$, indicating also the chemical stability of H$_2$O$_2$ under the present experimental conditions. Thus, H$_2$O$_2$ degradation was completely dependent on cellular mechanisms. Comparing the experiments shown in Figure 6A and C with those in Figures 3 and 5, we conclude that production and degradation of H$_2$O$_2$ are working in parallel. Cellular degradation of H$_2$O$_2$ seems to be triggered solely by critical [H$_2$O$_2$] and is obviously not directly stimulated by TPA or formyl peptides. The capacity of an MC to eliminate H$_2$O$_2$ with a high rate and covering a much larger area than the cell itself (Fig. 6C) may be of great importance to control local [H$_2$O$_2$] relevant for autocrine and paracrine signaling in neighboring cells.

Quantification of local [H$_2$O$_2$] decrease outside of 10 MCs similar to the ones shown in Figure 6A and C revealed that the [H$_2$O$_2$] declined with rates between 1.7 and 6.6 nM per second. If degradation would not occur, single MCs would increase local extracellular [H$_2$O$_2$] not only by 1.4 nM (taken

from CA and CV experiments) but by 3.1 up to 8.0 nM per second. Similarly, the initial local [H_2O_2] increase by 3.4 nM per second after TPA stimulation could even reflect initial local [H_2O_2] increases of 10 nM per second.

Validation of single-cell H_2O_2 determinations using bulk measurements with other techniques

To validate single-cell extracellular H_2O_2 measurements performed with the *ElProScan* (Fig. 7A, B; $n = 5$–11), we determined H_2O_2 in cell populations using the fluorescence-based Amplex UltraRed assay (AUR; Fig. 7G, H) and an ESR-based method recently established in our laboratory (63) (Fig. 7D, E). For comparison of the respective techniques side by side, modifications of the ESR and AUR protocols were required. Signal changes in the AUR assay and the here applied spectroscopic method are irreversible, thus not allowing dynamic measurements. To circumvent this disadvantage, single time point determinations of H_2O_2 were performed (47) (see the Materials and Methods section for details), which allow conclusions about the reaction kinetics, but with reduced temporal resolution.

H_2O_2 measurements with all three approaches were conducted in parallel using MCs from the same blood donors. While the electrochemical recordings with the *ElProScan* were continuous (recording of 1 Hz) and always from one single MC, ESR- and AUR-based H_2O_2 determinations reflect values at selected time points, representing about 25,000 MCs per point. When stimulated with TPA, cells in suspension as well as the electrochemically measured single cells responded with H_2O_2 production, revealing similar kinetics (black traces in Fig. 7A, D, G), which are not well time resolved in case of ESR and AUR. Application of H_2O_2 (10 μM) following TPA stimulation caused the signals to increase and subsequently to decline (red traces in Fig. 7A, D, G). The drop of the signals was triggered by H_2O_2 degradation processes of MCs and not by spontaneous chemical breakdown of H_2O_2 because cell-free experiments depicted in Figure 7 (red traces in C, F, I) revealed that [H_2O_2] was quite stable over 70 min under the experimental conditions used here.

Similar to TPA-stimulated MCs, unstimulated cells efficiently removed external H_2O_2 from the buffer (Fig. 7, red traces in B, E, H). The single-cell responses (Fig. 7: compare A and B and also Fig. 6A) demonstrate the individual characteristics of selected cells.

Addition of H_2O_2 to single cells or to MCs in suspension initially caused signal peaks, which, however, never reached the height of the peaks in the absence of cells. This was true for all three approaches (Fig. 7: compare A and B with C; D and E with F; and G and H with I). Two reasons may contribute to explain this effect: cells function as very effective sinks to absorb H_2O_2 and degrade it intracellularly, and in addition, H_2O_2-degrading enzymes (such as catalase) may be active in the extracellular space. Together, this explains reduced extracellular [H_2O_2] compared with cell-free buffer solution. Addition of catalase at the end of the cell-free AUR experiments completely blocked H_2O_2 signals, thereby confirming the specificity of the method (Fig. 7I).

In conclusion, cell population experiments validated the electrochemical single-cell measurements.

Discussion

Comprehensive understanding of inter-related physiological processes of auto- and paracrine H_2O_2 signaling (14, 21) requires real-time quantification of extracellular local [H_2O_2] kinetics originating from a single cell as presented here.

In recent studies, H_2O_2 has been predominantly determined in the extracellular space of cell populations with the fluorescence-based Amplex Red/Amplex UltraRed assays (25, 28, 41, 55, 62). Although it is possible to monitor H_2O_2 quite selectively in the subnanomolar range (47) and with some dynamics when using single time point determination (compare Fig. 7), the method has significant disadvantages (24, 68, 72). Most importantly, single-cell measurements and high temporal resolution are impossible and quantification is difficult.

Inside cells, genetically encoded fluorescent sensors such as HyPer variants (12, 13, 20, 57, 69), Orp1-roGFP2 (41, 48, 58), and roGFP2-Tsa2ΔCPΔCR (49) allow determinations of very low [H_2O_2], in part, with subcellular resolution. However, several problems are difficult to resolve: (i) Light can induce ROS generation. (ii) For measurement of [H_2O_2] dynamics, oxidized sensors (by H_2O_2) have to be reduced (recycled), for example, by intracellular glutathione and thioredoxins. Activities of these reductant mechanisms vary between cells and compartments and additionally depend on the metabolic state. Thus, precise quantification of [H_2O_2] would require quantification of endogenous redox capabilities of individual cells. (iii) Sensors may change their properties inside cells compared with calibration conditions outside. (iv) Extracellular application of defined [H_2O_2] is not appropriate for intracellular calibration because H_2O_2 transport into cells is highly regulated and can establish outside:inside gradients varying from 7:1 up to 650:1 (5, 27). In addition, H_2O_2 is effectively degraded in- and outside of cells [compare Figs. 6 and 7 and (66)]. (v) It cannot be excluded that transfection of cells using any vector may disturb physiological functioning of the cell, even when not directly visible.

For electrochemical H_2O_2 determination in the extracellular space of single cells, some excellent studies have been conducted using either nanotube arrays (31) or UMEs in the bare state or coated with different materials. A scanning electron microscope, very similar to our *ElProScan*, was used in these studies to monitor ROS and reactive nitrogen species (RNS) from single cells [*e.g.*, (2, 3)]. Applying different voltammetric and amperometric methods, including biological scanning electrochemical microscopy, currents elicited by low [H_2O_2] have been measured with considerable temporal and spatial resolution (10, 30, 42, 56). However, quantification of real-time dynamic changes in [H_2O_2] due to physiologically relevant production and degradation by single primary cells of human origin (*ex vivo*) has not been performed.

Combining a bare disk platinum UME with different voltammetric and amperometric techniques, we found chronoamperometry to be the method of choice to achieve the following goals: specificity for H_2O_2, quantification of dynamic [H_2O_2] changes in the physiologically relevant nanomolar range and stable (without UME fouling) long-term monitoring of H_2O_2 production and removal in the extracellular space right at the plasma membrane of a single cell.

Our local measurements report real-time [H$_2$O$_2$] changes above the intact whole cell body and can be easily calibrated for each measuring point at a temporal resolution of at least 1 Hz. Furthermore, production of H$_2$O$_2$ by a single human MC can be separated from concomitant degradation of H$_2$O$_2$ by the same cell.

Covering three up to six orders of magnitude of [H$_2$O$_2$], our electrochemical methods include the full physiological concentration range compared with usually only one order of magnitude reported for the genetically encoded fluorescent sensors. Chronoamperometry (CA) offers the best temporal resolution (≥ 1 Hz) over several hours, whereas with SWV, the best sensitivity can be achieved down to 5 nM [H$_2$O$_2$]. With the here applied electrochemical techniques, [H$_2$O$_2$] changes over time are determined about 5–8 μm above a single cell as a change in current (ΔI_{650}) within the active volume around the UME tip. These local changes are not detectable tens of micrometers distant from the cell in the bulk solution. Therefore, increasing and decreasing current values at the UME tip directly reflect local [H$_2$O$_2$] changes caused by a single cell. Using CA to measure single human MCs, we determined an average local [H$_2$O$_2$] increase of 3.4 nM per second in the first ($=$maximal) H$_2$O$_2$ production phase after TPA stimulation. If concomitant H$_2$O$_2$ degradation was taken into account, local [H$_2$O$_2$] increases as high as 10 nM per second were estimated.

In addition to single cells, the technology is, in principle, also applicable for extracellular [H$_2$O$_2$] recordings in intact tissues or isolated organs if accessible by the electrode.

However, there are also disadvantages of the electrochemical H$_2$O$_2$ measurements presented here: only the least sensitive CA method provides a sufficient time resolution ≥ 1 Hz. While the more sensitive SWV, CV, and LSV can resolve [H$_2$O$_2$] as low as 5 or 50 nM, respectively, their time resolution is more limited. In addition, SWV experiments, when conducted over ≥ 1 h, caused marked desensitization and finally the ruin of the electrode. Whether precoverage of the platinum wire with protective material, as described by other groups (2, 8) or other applications, could avoid these problems has to be elaborated in future. Finally, scanning electrochemical microscopy, as presented here, enables only measurements of extracellular H$_2$O$_2$, which could, however, be considered an advantage in case effects of H$_2$O$_2$ on receptors, ion channels (15), or intercellular signaling are to be studied. It is, however, a disadvantage if intracellular [H$_2$O$_2$] measurements are required. Already in 2012, Wang *et al.* (67) described an electrochemical technique to determine ROS and RNS also inside cultured cells with nanoelectrodes, a method that was also applied more recently by Actis *et al.*, 2014 (1). However, our UME of 10 μm ø cannot be used for intracellular measurements because it is too large to be impaled into MCs or cells of comparable size.

While temporal resolution of CA is very high, spatial resolution exemplarily shown in 2D scannings of single MCs (Figs. 3, 5, and 6) is in the low micrometer range and thus not as good as for genetically encoded fluorescent sensors, which are only limited by optical resolution.

To understand the redox physiology in more detail, especially in immune cells, a variety of ROS and RNS (such as ONOO$^-$) as well as other metabolites (such as H$_2$S) have to be considered in future (4). Further development of the setup and measuring protocols are necessary to electrochemically determine the abovementioned species with similar standard as for H$_2$O$_2$.

In summary, SWV, CV, LSV, and CA allow quantification of extracellular local [H$_2$O$_2$] kinetics originating from single cells. SWV offers the highest sensitivity, but is compromised by relatively low temporal resolution and irreversible UME destruction, which exclude reliable cell measurements over extended times. CV and LSV have a slightly reduced sensitivity and also a relatively low temporal resolution, but due to electrode cleaning procedures, UMEs can be used over extended times. In contrast to voltammetric methods, CA shows the lowest sensitivity for H$_2$O$_2$. However, it is sufficient for quantification of physiologically relevant extracellular local [H$_2$O$_2$] kinetics originating from single cells. In addition, CA offers stable long-term measurements with the best temporal resolution.

Materials and Methods

Materials were purchased from [A]Sigma-Aldrich; [B]Gibco; [C]Life Technologies/Molecular Probes; [D]Noxygen; [E]Promocell; [F]Merck; and [G]Becton-Dickinson BD (all in Germany).

Solutions

Dulbecco's PBS-I[A] (PBS-I), containing (mM) NaCl: 136.9; KCl: 2.68; CaCl$_2$: 0.905; MgCl$_2$: 0.49; KH$_2$PO$_4$: 1.47; and Na$_2$HPO$_4$: 8.1/enriched with glucose, 5 mM, pH 7.4 $\pm$ 0.03, 288 $\pm$ 1 mOsm; *LB* Medium[G] (for culture of *E. coli*) containing (g/L) tryptone: 10; NaCl: 10; and yeast extract: 5; and RPMI 1640-Medium[B] (+ 10% FCS +1% antibiotics pen/strep) were used.

Chemicals

Agarose[A], Amplex UltraRed Reagent[C] (dissolved in DMSO), catalase[A] (from bovine liver, 2000–5000 U/mg protein, freshly dissolved in PBS-I), CMH[D] (1-hydroxy-3-methoxycarbonyl-2,2,5,5-tetramethylpyrrolidine hydrochloride; dissolved in anoxic A. dest. +25 μM DF +5 μM DETC), DETC[D] (Na-diethyldithiocarbamate, dissolved in A. dest.), DF[D] (deferoxamine methanesulfonate salt, dissolved in A. dest.), DMSO[A] (dimethyl sulfoxide), FCS[B] (fetal calf serum), ferrocene methanol[A] (1 mM in 100 mM KCl), glucose[F], HRP[A] (horseradish peroxidase, Type VI-A, dissolved in A. dest.), and hydrogen peroxide[A] (30% w/w H$_2$O$_2$ stock solution; 9.8 M at 25°C; controlled by titration with KMnO$_4$) were used. From this stock, aliquots diluted with A. dest. were freshly prepared and stored in dark vials. KCl, KMnO$_4$[A], pen/strep[B] (penicillin 10 kU/mL/streptomycin 10 mg/mL), SOD[A] (superoxide dismutase, bovine, dissolved in PBS-I), TEMPOL[A] (4-hydroxy-TEMPO = 4-hydroxy-2,2,6,6-tetramethylpiperidine 1-oxyl; chemical oxidant; dissolved in A. dest.), TPA[A] (12-*O*-tetradecanoylphorbol-13-acetate, dissolved in DMSO), and VAS2870[A] (dissolved in DMSO) were used.

Other materials

Ultralow Attachment Surface Plates (*U-LASPs*, Corning/Costar) were used to keep cells in suspension. Dish used for electrochemical measurements was *FluoroDish*, sterile and with 35.5 mm $\times$ 10 mm/23 mm glass bottom (WPI). UMEs (disk platinum electrode, 10 μm ø) and electrode polishing

device *MHK1* (HEKA Elektronik Dr. Schulze GmbH) were used. Glass capillaries for ESR measurements were Ringcaps Pyrex (Hirschmann). Microplates for AUR measurements were black, 96-well, and with clear flat bottom (BD Falcon).

Preparation and culture of human MCs

The present research carried out with *ex vivo* leukocytes from anonymized healthy human blood donors (male/female) has been authorized by the local ethics committee in the declaration from April 16th, 2015 (84/15; Prof. Dr. Rettig-Stürmer). Out of use *leukocyte-reducing system chambers* were kindly provided by the local blood bank in the Department of Haemostaseology at Saarland University.

For preparation of human MCs, peripheral blood mononuclear cells were isolated, from which the MC population was separated following a selective adhesion protocol (57). MCs were cultured in RPMI medium (+ antibiotics) suspended in *U-LASPs* at 37°C in a humidified 5% CO_2 atmosphere for up to 25 days. For electrochemical experiments, cells (in RPMI medium) were plated at a density of 10^5 to 5×10^5 cells per dish at least 1 day before use and kept under culture conditions. Cells attach to the glass bottom within 1 h and eventually grow and differentiate to macrophages. Immediately before starting the experiment, attached MCs were washed twice with PBS-I and were measured in 2 mL of PBS-I. Dissolved effector substances were pipetted into the measuring buffer, followed by gentle mixing.

Electrochemical H_2O_2 measurements with the electrochemical probe scanner (ElProScan) ELP 3

The *ElProScan* system (HEKA Elektronik Dr. Schulze GmbH) working as a scanning electrochemical microscope (SECM) consists of three main components: (i) the controller *ESC 3* to control electrode and specimen positions; (ii) the amplifier *EPC 10 USB* (*Rev Y*) to generate voltage and measure current, connected to a 3-electrode head stage; and (iii) the positioning system with inverted microscope optics and CCD camera (*ProgRes, CapturePro 2.8.8, MFcool*; Jenoptik, Germany) for monochrome bright-field pictures.

The systems to drive specimen and UME positions, respectively, consist of a high-resolution 3-axis part (closed loop, linear optical encoder with 10-nm resolution; Applied Scientific Instrumentation) and an additional piezo translation stage on the *z*-axis (closed loop, linear optical encoder with 1.5-nm resolution; Physik Instrumente GmbH & Co. KG).

The inverted microscope optics is equipped with a tube lens (200 mm focus length), a motorized focus control (closed-loop rotary encoders with 5.5-nm resolution, bidirectional repeatability, SD <250 nm; Applied Scientific Instrumentation), and two objectives mounted on a nosepiece revolver: *LUCPLFLN* 40×, 0.6 N.A., WD 2.7-4 mm and *PLCN* 4×, 0.1 N.A. (both Olympus).

The equipment is mounted on a vibration-dampening table (TMC-Technical Manufacturing Corporation; sold by Qioptiq Photonics GmbH & Co. KG) and shielded in a *Faraday* cage (homemade), the front part of which is made up by a metal curtain (Ecologa Europe GmbH).

The 3-electrode setup consisted of the working (WE), the pseudoreference (RE; silver wire coated with AgCl), and the counter (CE; platinum wire) electrodes. For low-current measurements in the fA range, as needed for single-cell ex-

periments, the 2-electrode mode (WE + RE) turned out to be more favorable than the 3-electrode mode (+CE). An interface of polymerized agarose (5%) in KCl (3 M) to bridge the RE to the measuring buffer was tested: neither did it reduce current noise levels nor did it affect stability of long-time experiments (and was therefore not used).

A disk UME with a bare platinum wire of 10 μm ø and RG values of 1.6 - 3 [nomenclature for UME (7)] served as WE. RG is defined as the ratio between the insulator thickness (glass) and the radius of the platinum wire (here 5 μm). Electrochemical quality of a UME was routinely tested before starting a measurement. For that, cyclic voltammograms (CVs) in a potential window of -100 up to +400 mV (scan rate 50 mV/s) were recorded in ferrocene methanol (1 m*M* in KCl, 100 m*M*; *vs.* Ag/AgCl) solution. A UME was considered to be of high quality if a stable CV of low-noise current and a sigmoidal shape without significant hysteresis, but with long plateau phases at negative and higher positive potentials, were achieved (18, 33). Organic material adhering at the tip or other contaminations of the surface as well as partial damage of the tip are reflected by a worsening of the CV. Ultrasonic (for ≤10 s in ethanol, 70% followed by A. dest.; ultrasonic device *Sanitas*; Hans Dinslage GmbH) or mechanical cleaning of the tip with the *MHK1* electrode polisher frequently helped to improve the properties of the UME. For preconditioning of the UME before starting the measurement (and thereby shortening the run-in period) cleaning pulses were performed, which consisted of three repetitive potential steps (for 1 s, each) from 0 to +200 mV, then to -500 mV, and back to +200 mV.

Measurements were conducted at room temperature (RT) under constant white light and ambient air. Photographs of measured cells were routinely stored together with the experimental data. Single MCs attached to the bottom of the dish were approached by the electrode from above. The electrode positioning system of the setup measures the exact z-position of the UME tip with a resolution of <1 μm. The vertical distance between the tip and the cell is measured by the focus levels in the following way: after having approached the electrode about 20–30 μm above the cell, the height of the UME tip in focus and then the upper cell surface in focus are determined. Thereafter, the UME is slowly lowered and fixed 5–8 μm above the cell. Because of the irregular surface (microvilli *etc.*) of the cell, it is not possible to give a more precise value.

With an external standard device, the instrumental setup was routinely adjusted for amplification, capacitance, filters, and other parameters (defined in the *ElProScan* manual).

For data acquisition and analysis, the *PATCHMASTER* software (versions 2x74 and 2x90.2) with *ELPROSCAN* and *IMAGING* extensions (HEKA) was used. The system allows amperometric 2D line and matrix scanning of a probe following a freely programmable protocol. Scanning electrochemical microscopy (SECM) uses chronoamperometric (at 650 mV) constant height 2D scans of steady velocity with a speed of 1-10 μm/s in alternate mode (meander scan). Under these conditions, the position of the UME is fixed and the table with the cell dish is moved. According to a predefined setting, a scan starts in the lower right corner of the selected scan area, and the current is measured every x to x+Δx nm while scanning along the *x*-axis; scan lines are separated by Δy nm in the y-direction.

The usual instrumental setting for chronoamperometry (CA) was current gain 50 mV/pA; filter (I) 15 Hz Bessel; filter (II) 100 Hz Bessel; and current sampling frequency was 1 kHz. Each second, 1000 sampled values were averaged, resulting in recordings with a time resolution of 1 Hz. For transient voltammetric techniques such as CV, LSV, and SWV, parameters were adapted as described for the respective experiments. CA measurements of H₂O₂ were performed at 650 mV; in CV and LSV, currents were sampled in selected potential windows and with varying scan rates, depending on the aim of the experiment. For SWV experiments, parameters were set as follows: start and end potential of -100 mV and +900 mV; amplitude of the steps was ±75 mV and duration of one step pair was $\tau = 2$ s. At a scan rate of 5 mV/s, a frequency of 0.5 Hz, and a potential increment of 10 mV on top of each positively directed step, current values were sampled from the last 10% of the plateau phase of each up- and downward peak. SWV experiments were analyzed in two alternative ways: after having defined the baseline of a peak curve of $I_{difference}$ ($I_{difference} = I_{forward} - I_{reverse}$; see Fig. 2B), integration of the area of the curve or, alternatively, Δcurrent (baseline to peak) was used to calibrate SWV (compare Fig. 2C, D). Both methods gave similar results. However, definition of the baseline is problematic when trace curves are not clearly developed (especially at low [H₂O₂]) or when more than one peak appears.

In SWV experiments, so far unused UMEs showed high sensitivity for low nanomolar [H₂O₂]; however, they lost sensitivity during continued measuring, irrespective of whether or not H₂O₂ was added. For higher [H₂O₂] of 50 μM up to 1 mM, continued loss in sensitivity did not impair the measurements. Decline of UME sensitivity for H₂O₂ with time, even under repetitive electrochemical cleaning, made all attempts impossible to calibrate SWV measurements. Obviously, adsorption of material at the surface of the UME tip and modifications of the platinum wire in even deeper layers are of particular complexity when SWV is used (53). Thus, restoration of a desensitized UME was not possible with ultrasonic or other established cleaning methods. Occasionally, after polishing with abrasive paper (using the *MHK-1* device), the electrode was usable again.

UME polarization, limits of detection and quantification. Upon applying any potential between the electrodes in PBS-I measuring buffer, polarization (2) of the UME along the so-called run-in period can be observed. Components of the buffer adsorb at the UME tip, which modify the active area of the UME and may influence charge transfer. Upon starting CA measurements at 650 mV, the run-in phase characterized by decreasing current values lasts 5–20 min before a steady-state current flow is approached. The time required for current stabilization differs for each individual UME and depends on its preconditioning. In 72 different CA experiments (with 10 different UMEs), current values (I_{650}) of the respective approximate linear steady-state phases (averaged over 5 min) were calculated to be 507.2 ± 22.5 fA (mean ± SEM; SD = 190.8 fA). The limits of detection and of quantification, both calculated on the basis of standard deviation of the steady-state blank current ($I_{blank} = 507.2 ± 190.8$ fA), are 572.4 fA (3 × SD_blank) and 954 fA (5 × SD_blank), respectively (61).

Starting potential effect on sensitivity of voltammetric H₂O₂ determinations. Along with calibration experiments for H₂O₂ using CV, LSV, or SWV, it turned out that the starting potential was of crucial importance for the sensitivity of the UME. End potential was always +1.0 V. The current, sampled at 650 mV (I_{650}; where anodic oxidation of H₂O₂ occurs), gradually increased as the starting potential (beginning at +30 mV) moved into the negative direction. The effect reached its optimal plateau at potentials between -50 mV and -100 mV. The same was true for LSV experiments. In LSV, however, after jumping back from the end to the starting potential, the latter had to be clamped for at least 2 s before starting a new sweep. Obviously, within the above described critical potential interval, effective electrochemical cleaning of the electrode surface occurs due to desorption phenomena, thus yielding enhanced sensitivity toward H₂O₂ detection. As a consequence, for voltammetric experiments such as CV, LSV, and SWV, the starting potential was set to -100 mV (compare Figs. 1A, B, and 2B).

Generation of H₂O₂ at the UME along the ORR. As shown in Figure 1, voltammetric (CV, LSV) calibration experiments for H₂O₂ could be complicated when starting from -1.0 V. Current values (I_{650}) were even higher than expected for the deliberately added H₂O₂ to the buffer solution (black lines in Fig. 1D, E). At potentials more negative than -100 mV, the electrode reduction of dissolved oxygen is forming measurable amounts of H₂O₂ (due to $O_2 + 2H^+ + 2e^- \rightarrow H_2O_2$) (22, 59, 75). In an unstirred solution, this increases [H₂O₂] near the electrode above average values in the bulk. Consequently, current values (I_{650}) rise over time in the course of a repetitive CV experiment within the potential window from -1.0 V to +1.0 V. Adding H₂O₂ (10 μM) to the buffer resulted in a further increase of current. Conducting similar CV experiments in the presence of the enzyme catalase (∼400 U/mL), which causes dismutation of H₂O₂, no increase of current was seen neither before nor after extra application of H₂O₂. If those long-term CV measurements, however, were started at a potential of -100 mV (up to +1.0 V), no H₂O₂ production was measurable. Upon addition of H₂O₂, however, the expected current jump was observed (not shown).

Although oxygen can be reduced at Pt electrodes (*vs.* Ag/AgCl; neutral pH) at negative potentials starting from 0 V already (unpublished observations), this effect was not visible in our CV experiments. We suggest the following explanations for this discrepancy: The amount of H₂O₂ being produced at the slightly negative potential range between 0 and -100 mV cannot be high since this range is quickly changed toward positive potentials in CV. In addition, for production (at −100 mV) and measurement (at 650 mV) of H₂O₂ within one CV, the same UME is used. For measurement, H₂O₂ is oxidized at the electrode, thus preventing accumulation of H₂O₂ at the tip (59). Furthermore, due to the duration of one CV (at 50 mV/s) of >20 s, parts of H₂O₂ produced at the UME may have diffused away. Fundamental details about ORR are provided elsewhere (29).

Nevertheless, our results support the conclusion that at -100 mV, repetitive electrochemical cleaning of the electrode surface in CV (and LSV) is the reason for increased sensitivity rather than electrochemical formation of additional H₂O₂ due to ORR. The cleaning pulses for preconditioning

of the UME, which are mentioned above, hint in the same direction.

H_2O_2 measurements with ESR spectroscopy

An *ESP300* spectrometer (Bruker) equipped with a *TMH8603* cavity was used. ESR samples were transferred to 50-μl glass capillaries and measured at RT. For H_2O_2 determinations in MC suspensions, the hydroxylamine spin probe CMH was used, which served as an electron donor for the horseradish peroxidase-catalyzed reduction of H_2O_2, forming two CM radicals accessible by ESR (63). For the measurements, suspended MCs ($\geq$5 days after isolation) were washed in PBS-I, followed by centrifugation (RT, 220 g, 10 min). Then, four samples, each containing about 0.5 Mio cells/mL PBS-I, were differently treated following the protocol described in Figure 7. At selected time points, a 150-μL aliquot of each sample was taken and cells were spun down for 1 min at 14,200 g. From the supernatant, 50 μL was added to 50 μL measuring solution containing horseradish peroxidase (HRP) and CMH at final concentrations of 100 U/mL and 1 mM, respectively. Fifty microliters of this mixture was transferred to a glass capillary, and ESR spectra were measured. ESR parameters were set to a microwave power of 20 mW, a frequency of 9.5 GHz, a magnetic flux density of 0.3445 T, a sweep width of 6 mT, and modulation amplitude of 0.1 mT. The duration of one scan was 1 min with a time constant of 20 ms. TEMPOL (100 μM) served as a reference substance. The peak-to-peak height of the signals is proportional to the CM-radical concentration and hence to the [H_2O_2]. To ensure that reduction of H_2O_2 by HRP was complete at each time point of its determination, follow-up scans were checked for termination of the reaction. Experiments without cells (Fig. 7F) were conducted in the same way. Additional control experiments in the presence and absence of HRP, respectively, confirmed that exclusively H_2O_2, but not $\bullet O_2^-$, was measured. For calculations, the intensities of the ESR spectra were analyzed.

H_2O_2 measurements with the AUR assay

Measurements were conducted at RT in a microplate reader (*Infinite M 200 PRO*; Tecan, Germany). For the fluorometric determination of extracellular H_2O_2, MCs were used $\geq$5 days after isolation. Oxidation of the colorless nonfluorescent AUR to a fluorescent resorufin derivative by H_2O_2 is not reversible, thus allowing only endpoint determinations of [H_2O_2] in the solution. To follow the kinetics of the H_2O_2-producing and -degrading pathways of cells, the recommended measuring protocol for AUR was modified [(47) with description below]. MCs were prepared and treated as for ESR measurements and following the protocol described in Figure 7. At selected time points, 50 μL (in duplicate) of each sample (including about 25,000 cells) was added to 50 μL of measuring solution containing AUR and HRP at final concentrations of 30 μM and 0.1 U/mL, respectively (light-sensitive!). After having collected all samples of one respective time point in the microplate, it was immediately measured (bottom reading; gain 55; 9 reads per well; excitation at 535 nm/emission at 590 nm). The same procedure was applied for each time point of treatment as well as for the cell-free control samples.

Presentation and analyses of data; statistics

Cyclic and linear scan voltammogram presentations follow the IUPAC voltammogram convention with positive potential and anodic current in the positive *x*-axis and positive *y*-axis, respectively. For analysis of the experimental raw data, the standard accessory *PATCHMASTER* software (versions 2x74 and 2x90.2) of the measuring system was used. Further processing of data, statistics, and graphical presentations were carried out using *OriginPro 8.5G* and *CorelDRAW X4*. Values are mean $\pm$ SEM (or $\pm$ SD if explicitly stated).

Author Disclosure Statement

C.H. is employed at HEKA Elektronik Dr. Schulze GmbH, 67466 Lambrecht, Germany. All other authors declare no conflicting financial interests.

References

1. Actis P, Tokar S, Clausmeyer J, Babakinejad B, Mikhaleva S, Cornut R, Takahashi Y, Cordoba AL, Novak P, Shevchuck AI, Dougan JA, Kazarian SG, Gorelkin PV, Erofeev AS, Yaminsky IV, Unwin PR, Schuhmann W, Klenerman D, Rusakov DA, Sviderskaya EV, and Korchev YE. Electrochemical Nanoprobes for Single-Cell Analysis. *Acs Nano* 8: 875–884, 2014.

2. Amatore C, Arbault S, Bouton C, Drapier JC, Ghandour H, and Koh AC. Real-time amperometric analysis of reactive oxygen and nitrogen species released by single immunostimulated macrophages. *Chembiochem* 9: 1472–1480, 2008.

3. Amatore C, Arbault S, Bruce D, de Oliveira P, Erard M, and Vuillaume M. Characterization of the electrochemical oxidation of peroxynitrite: relevance to oxidative stress bursts measured at the single cell level. *Chemistry* 7: 4171–4179, 2001.

4. Amatore C, Arbault S, Guille M, and Lemaître F. Electrochemical monitoring of single cell secretion: vesicular exocytosis and oxidative stress. *Chem Rev* 108: 2585–2621, 2008.

5. Antunes F and Cadenas E. Estimation of H_2O_2 gradients across biomembranes. *Febs Lett* 475: 121–126, 2000.

6. Aon MA, Cortassa S, and O'Rourke B. Redox-optimized ROS balance: a unifying hypothesis. *Biochim Biophys Acta* 1797: 865–877, 2010.

7. Bard AJ and Faulkner LR. *Electrochemical Methods: Fundamentals and Applications, 2nd Edition.* New York, NY: John Wiley & Sons, 2000, p. 850.

8. Beaulieu I, Kuss S, Mauzeroll J, and Geissler M. Biological scanning electrochemical microscopy and its application to live cell studies. *Anal Chem* 83: 1485–1492, 2011.

9. Belousov VV, Fradkov AF, Lukyanov KA, Staroverov DB, Shakhbazov KS, Terskikh AV, and Lukyanov S. Genetically encoded fluorescent indicator for intracellular hydrogen peroxide. *Nat Methods* 3: 281–286, 2006.

10. Bergner S, Vatsyayan P, and Matysik FM. Recent advances in high resolution scanning electrochemical microscopy of living cells—A review. *Anal Chim Acta* 775: 1–13, 2013.

11. Bienert GP and Chaumont F. Aquaporin-facilitated transmembrane diffusion of hydrogen peroxide. *Biochim Biophys Acta* 1840: 1596–1604, 2014.

12. Bilan DS and Belousov VV. HyPer Family Probes: state of the Art. *Antioxid Redox Signal* 24: 731–751, 2016.

13. Bilan DS, Pase L, Joosen L, Gorokhovatsky AY, Ermakova YG, Gadella TW, Grabher C, Schultz C, Lukyanov S, and Belousov VV. HyPer-3: a genetically encoded H$_2$O$_2$ probe with improved performance for ratiometric and fluorescence lifetime imaging. *ACS Chem Biol* 8: 535–542, 2013.

14. Bogeski I, Kummerow C, Al-Ansary D, Schwarz EC, Koehler R, Kozai D, Takahashi N, Peinelt C, Griesemer D, Bozem M, Mori Y, Hoth M, and Niemeyer BA. Differential redox regulation of ORAI ion channels: a mechanism to tune cellular calcium signaling. *Sci Signal* 3: ra24, 2010.

15. Bogeski I and Niemeyer BA. Redox regulation of ion channels. *Antioxid Redox Signal* 21: 859–862, 2014.

16. Brandes RP, Weissmann N, and Schröder K. Nox family NADPH oxidases: molecular mechanisms of activation. *Free Radic Biol Med* 76C: 208–226, 2014.

17. Bufe B, Schumann T, Kappl R, Bogeski I, Kummerow C, Podgorska M, Smola S, Hoth M, and Zufall F. Recognition of Bacterial Signal Peptides by Mammalian Formyl Peptide Receptors: a new mechanism for sensing pathogens. *J Biol Chem* 290: 7369–7387, 2015.

18. Danis L, Polcari D, Kwan A, Gateman SM, and Mauzeroll J. Fabrication of carbon, gold, platinum, silver, and mercury ultramicroelectrodes with controlled geometry. *Anal Chem* 87: 2565–2569, 2015.

19. Dikalov SI, Li W, Mehranpour P, Wang SS, and Zafari AM. Production of extracellular superoxide by human lymphoblast cell lines: comparison of electron spin resonance techniques and cytochrome C reduction assay. *Biochem Pharmacol* 73: 972–980, 2007.

20. Ermakova YG, Bilan DS, Matlashov ME, Mishina NM, Markvicheva KN, Subach OM, Subach FV, Bogeski I, Hoth M, Enikolopov G, and Belousov VV. Red fluorescent genetically encoded indicator for intracellular hydrogen peroxide. *Nat Commun* 5: 5222, 2014.

21. Forman HJ, Ursini F, and Maiorino M. An overview of mechanisms of redox signaling. *J Mol Cell Cardiol* 73: 2–9, 2014.

22. Gomez-Marin AM, Rizo R, and Feliu JM. Some reflections on the understanding of the oxygen reduction reaction at Pt(111). *Beilstein J Nanotechnol* 4: 956–967, 2013.

23. Gostner JM, Becker K, Fuchs D, and Sucher R. Redox regulation of the immune response. *Redox Rep* 18: 88–94, 2013.

24. Grisham MB. Methods to detect hydrogen peroxide in living cells: possibilities and pitfalls. *Comp Biochem Physiol A Mol Integr Physiol* 165: 429–438, 2013.

25. Guo H, Aleyasin H, Dickinson BC, Haskew-Layton RE, and Ratan RR. Recent advances in hydrogen peroxide imaging for biological applications. *Cell Biosci* 4: 64, 2014.

26. Hall SB, Khudaish EA, and Hart AL. Electrochemical oxidation of hydrogen peroxide at platinum electrodes. Part II: effect of potential. *Electrochim Acta* 43: 2015–2024, 1998.

27. Huang BK and Sikes HD. Quantifying intracellular hydrogen peroxide perturbations in terms of concentration. *Redox Biol* 2: 955–962, 2014.

28. Kalyanaraman B, Darley-Usmar V, Davies KJA, Dennery PA, Forman HJ, Grisham MB, Mann GE, Moore K, Roberts LJ, and Ischiropoulos H. Measuring reactive oxygen and nitrogen species with fluorescent probes: challenges and limitations. *Free Radic Biol Med* 52: 1–6, 2012.

29. Katsounaros I, Schneider WB, Meier JC, Benedikt U, Biedermann PU, Auer AA, and Mayrhofer KJ. Hydrogen peroxide electrochemistry on platinum: towards understanding the oxygen reduction reaction mechanism. *Phys Chem Chem Phys* 14: 7384–7391, 2012.

30. Kikuchi H, Prasad A, Matsuoka R, Aoyagi S, Matsue T, and Kasai S. Scanning Electrochemical Microscopy Imaging during Respiratory Burst in Human Cell. *Front Physiol* 7: 25, 2016.

31. Kim JH, Patra CR, Arkalgud JR, Boghossian AA, Zhang J, Han J H, Reuel NF, Ahn JH, Mukhopadhyay D, and Strano MS. Single-molecule detection of H$_2$O$_2$ mediating angiogenic redox signaling on fluorescent single-walled carbon nanotube array. *ACS Nano* 5: 7848–7857, 2011.

32. Kraaij MD, Koekkoek KM, van der Kooij SW, Gelderman KA, and van Kooten C. Subsets of human type 2 macrophages show differential capacity to produce reactive oxygen species. *Cell Immunol* 284: 1–8, 2013.

33. Kuss S, Cornut R, Beaulieu I, Mezour MA, Annabi B, and Mauzeroll J. Assessing multidrug resistance protein 1-mediated function in cancer cell multidrug resistance by scanning electrochemical microscopy and flow cytometry. *Bioelectrochemistry* 82: 29–37, 2011.

34. Kwon MJ, Lee KY, Lee HW, Kim JH, and Kim TY. SOD3 Variant, R213G, Altered SOD3 Function, Leading to ROS-Mediated Inflammation and Damage in Multiple Organs of Premature Aging Mice. *Antioxid Redox Signal* 23: 985–999, 2015.

35. Largeaud F, Kokoh KB, Beden B, and Lamy C. On the Electrochemical Reactivity of Anomers - Electrocatalytic Oxidation of Alpha-D-Glucose and Beta-D-Glucose on Platinum-Electrodes in Acid and Basic-Media. *J Electroanal Chem* 397: 261–269, 1995.

36. Lennicke C, Rahn J, Lichtenfels R, Wessjohann LA, and Seliger B. Hydrogen peroxide - production, fate and role in redox signaling of tumor cells. *Cell Commun Signal* 13: 39, 2015.

37. Li Y, Kim JG, Kim HJ, Moon MY, Lee JY, Kim J, Kim SC, Song DK, Kim YS, and Park JB. Small GTPases Rap1 and RhoA regulate superoxide formation by Rac1 GTPases activation during the phagocytosis of IgG-opsonized zymosans in macrophages. *Free Radic Biol Med* 52: 1796–1805, 2012.

38. Li Y, Sella C, Lemaître F, Guille-Collignon M, Thouin L, and Amatore C. Highly Sensitive Platinum-Black Coated Platinum Electrodes for Electrochemical Detection of Hydrogen Peroxide and Nitrite in Microchannel. *Electroanalysis* 25: 895–902, 2013.

39. Liu XP and Zweier JL. A real-time electrochemical technique for measurement of cellular hydrogen peroxide

generation and consumption: evaluation in human polymorphonuclear leukocytes. *Free Radic Biol Med* 31: 894–901, 2001.

40. Lukyanov KA and Belousov VV. Genetically encoded fluorescent redox sensors. *Biochim Biophys Acta* 1840: 745–756, 2014.

41. Maghzal GJ, Krause KH, Stocker R, and Jaquet V. Detection of reactive oxygen species derived from the family of NOX NADPH oxidases. *Free Radic Biol Med* 53: 1903–1918, 2012.

42. Matsue T. Bioimaging with Micro/Nanoelectrode Systems. *Anal Sci* 29: 171–179, 2013.

43. Migeotte I, Communi D, and Parmentier M. Formyl peptide receptors: a promiscuous subfamily of G protein-coupled receptors controlling immune responses. *Cytokine Growth Factor Rev* 17: 501–519, 2006.

44. Mirceski V, Gulaboski R, Lovric M, Bogeski I, Kappl R, and Hoth M. Square-Wave Voltammetry: a Review on the Recent Progress. *Electroanalysis* 25: 2411–2422, 2013.

45. Mirceski V, Guziejewski D, Bozem M, and Bogeski I. Characterizing electrode reactions by multisampling the current in square-wave voltammetry. *Electrochim Acta* 213: 520–528, 2016.

46. Mirceski V, Guziejewski D, and Gulaboski R. Electrode Kinetics from a Single Square-Wave Voltammogram. *Macedonian J Chem Chem Eng* 34: 181–188, 2015.

47. Mishin V, Gray JP, Heck DE, Laskin DL, and Laskin JD. Application of the Amplex red/horseradish peroxidase assay to measure hydrogen peroxide generation by recombinant microsomal enzymes. *Free Radic Biol Med* 48: 1485–1491, 2010.

48. Morgan B, Sobotta MC, and Dick TP. Measuring E_{GSH} and H_2O_2 with roGFP2-based redox probes. *Free Radic Biol Med* 51: 1943–1951, 2011.

49. Morgan B, Van Laer K, Owusu TN, Ezerina D, Pastor-Flores D, Amponsah PS, Tursch A, and Dick TP. Real-time monitoring of basal H_2O_2 levels with peroxiredoxin-based probes. *Nat Chem Biol* 12: 437–443, 2016.

50. Murray PJ, Allen JE, Biswas SK, Fisher EA, Gilroy DW, Goerdt S, Gordon S, Hamilton JA, Ivashkiv LB, Lawrence T, Locati M, Mantovani A, Martinez FO, Mege JL, Mosser DM, Natoli G, Saeij JP, Schultze JL, Shirey KA, Sica A, Suttles J, Udalova I, van Ginderachter JA, Vogel SN, and Wynn TA. Macrophage Activation and Polarization: nomenclature and Experimental Guidelines. *Immunity* 41: 14–20, 2014.

51. Musset B, Cherny VV, and DeCoursey TE. Strong glucose dependence of electron current in human monocytes. *Am J Physiol Cell Physiol* 302: C286–C295, 2012.

52. Nauseef WM. Detection of superoxide anion and hydrogen peroxide production by cellular NADPH oxidases. *Biochim Biophys Acta* 1840: 757–767, 2014.

53. Norouzi P, Garakani TM, Rashedi H, Zamani HA, and Ganjali MR. Ultrasensitive Flow-Injection Electrochemical Method Using Fast Fourier Transform Square-Wave Voltammetry for Detection of Vitamin B-1. *Int J Electrochem Sci* 5: 639–652, 2010.

54. Petry A, Weitnauer M, and Gorlach A. Receptor Activation of NADPH Oxidases. *Antioxid Redox Signal* 13: 467–487, 2010.

55. Rhee SG, Chang TS, Jeong W, and Kang D. Methods for detection and measurement of hydrogen peroxide inside and outside of cells. *Mol Cells* 29: 539–549, 2010.

56. Roberts WS, Lonsdale DJ, Griffiths J, and Higson SP. Advances in the application of scanning electrochemical microscopy to bioanalytical systems. *Biosens Bioelectron* 23: 301–318, 2007.

57. Saul S, Gibhardt CS, Schmidt B, Lis A, Pasieka B, Conrad D, Jung P, Gaupp R, Wonnenberg B, Diler E, Stanisz H, Vogt T, Schwarz EC, Bischoff M, Herrmann M, Tschernig T, Kappl R, Rieger H, Niemeyer BA, and Bogeski I. A calcium-redox feedback loop controls human monocyte immune responses: the role of ORAI Ca^{2+} channels. *Sci Signal* 9: ra26, 2016.

58. Schwarzländer M, Dick TP, Meyer AJ, and Morgan B. Dissecting Redox Biology Using Fluorescent Protein Sensors. *Antioxid Redox Signal* 24: 680–712, 2016.

59. Shen Y, Trauble M, and Wittstock G. Detection of hydrogen peroxide produced during electrochemical oxygen reduction using scanning electrochemical microscopy. *Anal Chem* 80: 750–759, 2008.

60. Shi C and Pamer EG. Monocyte recruitment during infection and inflammation. *Nat Rev Immunol* 11: 762–774, 2011.

61. Shrivastava A and Gupta V. Methods for the determination of limit of detection and limit of quantitation of the analytical methods. *Chronicles Young Sci* 2: 21, 2011.

62. Soh N. Recent advances in fluorescent probes for the detection of reactive oxygen species. *Anal Bioanal Chem* 386: 532–543, 2006.

63. Thierbach S, Bui N, Zapp J, Chhabra SR, Kappl R, and Fetzner S. Substrate-assisted O_2 activation in a cofactor-independent dioxygenase. *Chem Biol* 21: 217–225, 2014.

64. Triggiani M, Petraroli A, Loffredo S, Frattini A, Granata F, Morabito P, Staiano RI, Secondo A, Annunziato L, and Marone G. Differentiation of monocytes into macrophages induces the upregulation of histamine H1 receptor. *J Allergy Clin Immunol* 119: 472–481, 2007.

65. Urbach HB and Bowen RJ. Behaviour of Oxygen-Peroxide Couple on Platinum. *Electrochim Acta* 14: 927–940, 1969.

66. Wagner BA, Witmer JR, van 't Erve TJ, Buettner GR. An assay for the rate of removal of extracellular hydrogen peroxide by cells. *Redox Biol* 1: 210–217, 2013.

67. Wang YX, Noel JM, Velmurugan J, Nogala W, Mirkin MV, Lu C, Collignon MG, Lemaître F, and Amatore C. Nanoelectrodes for determination of reactive oxygen and nitrogen species inside murine macrophages. *Proc Natl Acad Sci U S A* 109: 11534–11539, 2012.

68. Wardman P. Fluorescent and luminescent probes for measurement of oxidative and nitrosative species in cells and tissues: progress, pitfalls, and prospects. *Free Radic Biol Med* 43: 995–1022, 2007.

69. Warren EAK, Netterfield TS, Sarkar S, Kemp ML, and Payne CK. Spatially-resolved intracellular sensing of hydrogen peroxide in living cells. *Sci Rep* 5: 16929, 2015.

70. Winterbourn CC. Reconciling the chemistry and biology of reactive oxygen species. *Nat Chem Biol* 4: 278–286, 2008.

71. Winterbourn CC. The biological chemistry of hydrogen peroxide. *Methods Enzymol* 528: 3–25, 2013.

72. Winterbourn CC. The challenges of using fluorescent probes to detect and quantify specific reactive oxygen species in living cells. *Biochim Biophys Acta* 1840: 730–738, 2014.

73. Winterbourn CC and Hampton MB. Thiol chemistry and specificity in redox signaling. *Free Radic Biol Med* 45: 549–561, 2008.

74. Zhang Y and Wilson GS. Electrochemical Oxidation of H$_2$O$_2$ on Pt and Pt + Ir Electrodes in Physiological Buffer and Its Applicability to H$_2$O$_2$-Based Biosensors. *J Electroanal Chem* 345: 253–271, 1993.

75. Zhou M, Yu Y, Hu K, and Mirkin MV. Nanoelectrochemical approach to detecting short-lived intermediates of electrocatalytic oxygen reduction. *J Am Chem Soc* 137: 6517–6523, 2015.

Address correspondence to:
Dr. Monika Bozem
Department of Biophysics
Faculty of Medicine
Center for Integrated Physiology
and Molecular Medicine (CIPMM)
Saarland University
Homburg 66421
Germany

E-mail: monika.bozem@uks.eu

Prof. Markus Hoth
Department of Biophysics
Faculty of Medicine
Center for Integrated Physiology
and Molecular Medicine (CIPMM)
Saarland University
Homburg 66421
Germany

E-mail: markus.hoth@uks.eu

Abbreviations Used

AUR = Amplex® UltraRed
CA = chronoamperometry
CMH = 1-hydroxy-3-methoxycarbonyl-2,2,5,5-tetramethylpyrrolidine hydrochloride
CV = cyclic voltammetry, cyclic voltammogram
DMSO = dimethyl sulfoxide
ElProScan = electrochemical probe scanner
ESR = electron spin resonance
[H$_2$O$_2$] = local concentration of hydrogen peroxide
HRP = horseradish peroxidase
LSV = linear scan voltammetry, linear scan voltammogram
MPh = macrophage
MC = monocyte
NO$^{\bullet}$ = nitric oxide
NOX = NADPH oxidase
$^{\bullet}$O$_2^-$ = superoxide
ORR = oxygen reduction reaction
RNS = reactive nitrogen species
ROS = reactive oxygen species
SECM = scanning electrochemical microscope (microscopy)
SOD = superoxide dismutase
SWV = square wave voltammetry
TPA = 12-*O*-tetradecanoylphorbol-13-acetate
U-LASP = ultralow attachment surface plate
UME = ultramicroelectrode